Fuel 197 (2017) 58–69

Contents lists available at ScienceDirect

Fuel

journal homepage: www.elsevier.com/locate/fuel

Full Length Article

Foam flow in a layered, heterogeneous porous medium: A visualization study

Robin Singh, Kishore K. Mohanty *

Department of Petroleum and Geosystems Engineering, The University of Texas at Austin, Austin, TX 78712, United States

HIGHLIGHTS

- Nanoparticles increase foam stability in both bulk and porous media.
- Foam improves sweep efficiency with and without crude oil.
- High oil recoveries are observed in heterogeneous media due to immiscible foams.

GRAPHICAL ABSTRACT

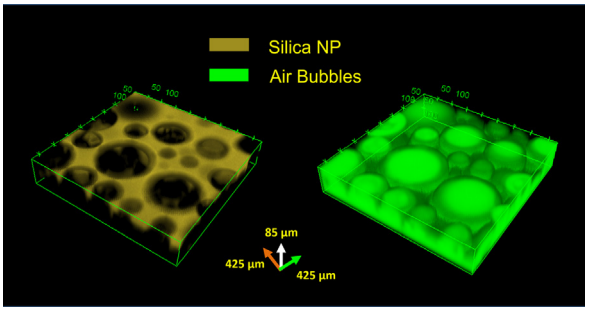

ARTICLE INFO

Article history:
Received 19 December 2016
Received in revised form 4 February 2017
Accepted 8 February 2017

Keywords:
Foam
Nanoparticle
Oil recovery
Heterogeneous porous media
Flow diversion

ABSTRACT

Foams can divert flow from high permeability regions to low permeability regions in heterogeneous porous media. In this work, we present a visualization study of foam flow through a two-layer, heterogeneous model, where the performance of foam stabilized by surfactant-nanoparticle mixtures is evaluated. An in-house, 2D sandpack holder was fabricated with a transparent front plate to visualize foam displacement mechanisms. It was packed with two layers of silica sand which resulted in a permeability contrast of 6:1. Foam flow and oil displacement experiments were performed using either surfactants or surfactant-nanoparticle blends. Foam flow experiments revealed that inclusion of nanoparticles increases the resistance factor (RF) by a factor of 1.95 over that of the surfactant foams. In oil displacement experiments, the water flood recoveries were low (~46% of the original-oil-in-place, OOIP) due to channeling through the top high-permeability region, leaving the bottom low-permeability region completely unswept. Foam flooding with an immiscible gas led to an improvement in sweep efficiency and resulted in an oil recovery as high as 80% OOIP. Foams stabilized by the surfactant-nanoparticle blend outperform surfactant-stabilized foams by 9% OOIP incremental oil. This study is the first-of-its-kind to visually demonstrate flow diversion due to nanoparticle-stabilized foam in a heterogeneous, porous system. Flow phenomena such as cross-flow between layers and foam phase separation are discussed. Complementary experiments such as static foam tests and confocal laser scanning microscopy are also performed to understand the effect of nanoparticles on foam stability.

1. Introduction

Gas flooding has been commercially applied as an enhanced oil recovery technique for nearly 50 years. Based on a 2014 survey, US CO_2-EOR projects alone provide 292,735 barrels of oil per day, which accounts for 38% of US output from EOR [1]. This technique involves the injection of a gas (e.g., hydrocarbon components like methane, ethane and enriched-gases, and non-hydrocarbon components like carbon dioxide, nitrogen, and flue gas) into the oil reservoirs. These injected gases are either immiscible, partially miscible, or completely miscible with the reservoir

* Corresponding author.
E-mail address: mohanty@mail.utexas.edu (K.K. Mohanty).

http://dx.doi.org/10.1016/j.fuel.2017.02.019
0016-2361/

crude oil. One of the advantages of gas flooding is better microscopic displacement efficiency which results in lowering of residual oil saturation as compared to waterflood [2]. However, the volumetric sweep efficiency is often very poor due to the inherent lower viscosity and density of the gas which leads to viscous fingering and gravity override, respectively [3]. The other main technical issue is the channeling of gas through high permeability regions in a heterogeneous reservoir. These technical challenges result in an early gas breakthrough, poor sweep efficiency, and inefficient oil recovery.

Foam is a potential solution to alleviate these above-mentioned challenges associated with gas flooding [4,5]. It can drastically reduce the gas mobility by several orders of magnitude by increasing the apparent viscosity of gas and trapping a large gas fraction inside the porous medium [6]. In the past, there have been several field tests, e.g., steam foam flood [7], foam-assisted water-alternating-gas injection [8], carbon dioxide foam flood [9], and foam flood with a carbon dioxide-soluble surfactant [10] in which foam was used to improve sweep efficiency. Conventionally, surfactants have been used to stabilize foam in the field application. However, surfactant-stabilized foams are not very stable under harsh reservoir condition such as high temperature, high salinity, and in the presence of crude oil [11]. The other factors such as surfactant adsorption on rock matrix, surfactant-partitioning in crude oil, thermal degradation of surfactant under high temperature further pose challenges toward economical field implementation of foam flooding [12–14].

The use of nanoparticles can help mitigate some of these issues [15]. Nanoparticles have the potential to stabilize foam under harsh conditions of temperature, salinity, presence of crude oil. Moreover, these nanoparticles can be obtained cost effectively from cheap raw materials like fly ash and silica [16,17]. Surface-modified silica nanoparticles with varying degree of hydrophobicity have been shown to stabilize bulk foam even in the absence of any other surface-active agents such as surfactant [18,19]. Yu et al. [20] demonstrated that nanosilica-stabilized CO_2 foam improved the apparent viscosity of gas by a factor of 2–11 in their capillary flow experiments.

The modulation of nanoparticle surfaces via chemical treatment can sometimes be expensive. In such cases, an easier, cost-effective, and versatile approach is to modulate the surface property of these particles by in situ adsorption of surfactants on their surfaces. Gonzenbach et al. (2006) reported a versatile approach to prepare ultra-stable particle-stabilized bulk foams which were stable for the order of several days [21]. The nanoparticle surface was in-situ hydrophobized by adsorption of short-chain amphiphilic molecules which rendered them partially hydrophobic. Arriaga et al. (2012) employed a similar approach to study foaming properties of silica nanoparticles-amylamine mixtures [22]. They emphasized that by tuning the concentration of both species, different foam-regime can be obtained and to achieve ultra-stable foam sufficient concentration of both species is necessary. Zhu et al. (2015) demonstrated that bulk foam can be stabilized using negatively-charged silica nanoparticles hydrophobized in situ with a trace amount of a conventional cationic surfactant [23]. Recently, we showed that in-situ surface-activated nanoparticles behave as surfactants and could potentially be used as foaming agents in gas enhanced oil recovery (EOR) processes [15].

The concept of utilizing the synergistic interactions between nanoparticles and surfactant for foam stabilization is fairly new in the context of subsurface applications. Worthen et al. (2013) reported generation of stable and viscous CO_2-in-water foam with a fine texture in bead packs using bare colloidal silica and zwitterionic surfactant (caprylamidopropyl betaine) mixture when neither of these species could stabilize foam independently [24]. Sun et al. (2014) conducted several micromodel flooding experiments in which they showed that foam stabilized by silica nanoparticles-SDS blend can recover additional oil as compared to just SDS foam flood [25]. This additional recovery was attributed to enhance foam stability and viscoelasticity caused by the attached nanoparticles. Zargartalebi et al. (2015) studied foam stabilized NP-surfactant mixtures in homogenous sand packs [26]. They showed that the performance of surfactant-stabilized foam can be further augmented by inclusion of nanoparticles in the solution.

In our previous study [27], we investigated the synergistic effects of the mixture of hydrophilic silica nanoparticles and surfactant (α-olefin sulfonate) on foam stabilization in both bulk and homogeneous porous media. We demonstrated that as the concentration of nanoparticles increases, the mobility reduction factor of surfactant-NP foam in homogeneous Berea core increases up to a factor of two. Most of the reservoirs tend to be heterogeneous in nature, where volumetric sweep dominates the oil recovery process. The aspect of volumetric sweep improvement via foams cannot be investigated in a 1D homogenous core. Thus, it becomes vital to evaluate the volumetric sweep of nanoparticle-stabilized foams in heterogeneous and multi-dimensional systems. Moreover, a flow visualization study can offer insights into foam flow mechanisms such as cross-flow [28]. Keeping this in mind, we focused on visualization of foam flow in a two-layered system with a permeability contrast in this work. An in-house, 2D sandpack holder was fabricated with a transparent front plate to visualize foam flow processes. It was packed with two layers of silica sand — top layer with 40–70 mesh and bottom layer with 100–120 mesh, which resulted in a permeability contrast of 6:1. Aqueous foams were created in the sandpack in-situ by co-injecting the aqueous solution (with surfactant and/or nanoparticles) and the nitrogen gas at a fixed quality (gas volume fraction). The pressure drop across the sandpack was measured to estimate the achieved resistance factor (RF). This study is the first-of-its-kind to visually demonstrate flow diversion due to nanoparticle-stabilized foams, with or without crude oil, in a heterogeneous porous medium. Complementary bulk foam experiments such as static foam tests, confocal laser scanning microscopy were also performed to understand the effect of nanoparticles on foam stability.

2. Methodology

2.1. Materials

Commercially available silica nanoparticles, Nyacol DP 9711 used in this study was supplied by Nyacol Nano Technologies, Inc. Fluorescent silica nanoparticles (FL-NP) were obtained from 3M (St. Paul, MN) with a nominal diameter of 5 nm and polyethylene glycol (PEG) coating brings the particles to a nominal diameter of 10 nm. The anionic surfactant Bioterge AS-40, a C_{14-16} alpha-olefin sulfonate (AOS), (39% active) was provided by Stepan Co. This surfactant is considered a good foaming agent and has been extensively used in both lab-scale [11,27] and field-scale applications [7]. Sodium chloride (Fisher Chemical), and nitrogen (research grade, Matheson) was used as received. Ultrapure water with a resistivity greater than 18.2 MΩ-cm was used to prepare brine solutions. Blue food color (McCormick) was used to visualize the displacement of brine in foam flow experiments. Sand (US Silica) of two different mesh sizes- 100–120# and 40–70# were used to prepare heterogeneous sandpacks. Crude oil was obtained from a reservoir and it had a viscosity of 32 cp at 25 °C and density of 0.825 g/cm^3. The viscosity was measured using an AR-G2 rheometer from TA instruments.

2.2. Aqueous stability of nanoparticles

The silica nanoparticles used in this study have PEG-chains grafted to the surface which makes them hydrophilic in nature and prevents nanoparticles aggregation. Previous nanoparticle-transport studies have reported that the retention of these nanoparticles in porous media is very low [27,29]. The size of the nanoparticles was characterized using a Transmission Electron Microscope (TEM). A droplet of nanoparticle dispersion was placed on a Formvar-coated copper grid and was analyzed using FEI Tecnai TEM operating at 80 kV. The mean diameters of primary particles were found to be 20 nm via image analysis using Image J software. The TEM image is shown in Fig. 1. The particle hydrodynamic diameters in the aqueous dispersions were characterized via dynamic light scattering (DLS) technique using the Delsa™ Nano analyzer without any pH adjustment at room temperature.

The stock solutions of 2 wt% nanoparticles and 1 wt% Bioterge surfactant were first prepared. These stock solutions were used to prepare four samples containing varying concentrations of NaCl (1, 2, 4, 8 wt%) and 0.3 wt% nanoparticles mixed with 0.5 wt% surfactant. These dispersions were stirred for 24 h to ensure a homogeneous solution. Fig. 2 shows the solutions in vials after 6 months of preparation. A clear solution indicates no signs of precipitation and large shelf-lives of these formulations. Table 1 shows measured hydrodynamic diameter of the nanoparticles for these samples measured after six months of preparation. It is to be noted that using this technique we get the 'hydrodynamic' diameter and not the actual particle core-diameter (as measured by TEM). Typically, the DLS values are higher than TEM values as DLS technique is biased towards bigger particles in the solution [30].

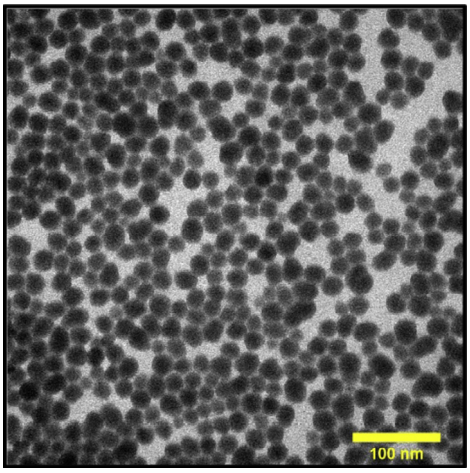

Fig. 1. TEM image of the Nyacol silica nanoparticle (Scale Bar is 100 nm).

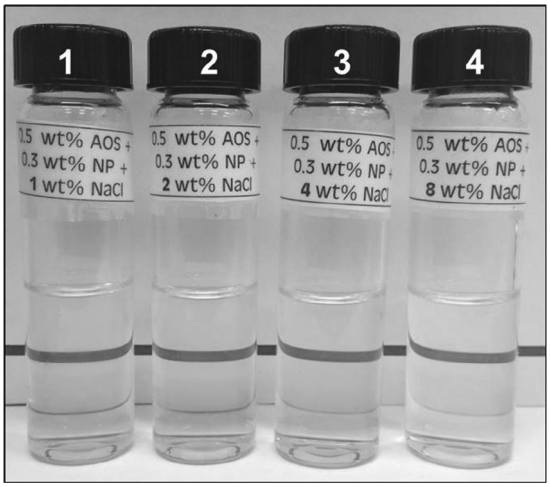

Fig. 2. Aqueous solutions containing 0.5 wt% AOS surfactant and 0.3 wt% NP with salinity of 1, 2, 4, 8 wt% NaCl (left to right).

Table 1
Hydrodynamic diameter of NP as measured by dynamic light scattering technique.

Label	Sample	Hydrodynamic diameter (nm)
1	0.5 wt% AOS + 0.3 wt% NP + 1 wt% NaCl	27.6 ± 7
2	0.5 wt% AOS + 0.3 wt% NP + 2 wt% NaCl	23.4 ± 6.9
3	0.5 wt% AOS + 0.3 wt% NP + 4 wt% NaCl	27.8 ± 6.4
4	0.5 wt% AOS + 0.3 wt% NP + 8 wt% NaCl	30.7 ± 7.1

2.3. Static foam tests

Bulk foam stability experiments are usually conducted as a screening tool to select foaming formulation for porous media application. One of such common experiments is the static foam test [11,27,31]. Recently, Jones et al. (2016) reported a good correlation between bulk foam stability and apparent foam viscosity in the absence of oil [32]. Similar tests were performed in this study to investigate the effect of nanoparticles on bulk foam stabilized by the surfactant-nanoparticle mixture. The setup consisted of a transparent graduated cylinder made of acrylic (diameter: 1 cm, length: 20 cm) with a stainless steel sparging frit (pore size 2 μm; Supelco, PA) at the bottom, which was used to inject air. Both ends of the cylinder were sealed using Swagelok fittings to prevent evaporation. First, 20 ml of sample was then taken in the cylinder and then the whole system was placed in the oven (55 °C or 75 °C) for more than 2 h to attain thermal equilibrium. Then, the air was injected at a constant pressure of 2 psi from the bottom generating static foam with a fine texture. The height of the foam (above the liquid phase) was monitored as a function of time. Half-life, which is the time for the volume of foam to be reduced to half of its original volume, was calculated for each case.

2.4. Confocal laser scanning microscopy (CLSM)

CLSM was performed using a Leica SP2 AOBS Confocal Microscope with the 10X dry (HC PL APO 0.40NA CS) objective lens operating in fluorescence mode. Fluorescent silica nanoparticles (FL-NP) used were visible under fluorescence microscopy when excited with 488 nm wavelength laser. 10 ml of an aqueous formulation containing 0.5 wt% surfactant and 0.3 wt% FL-NP was taken in a glass vial and was hand-shaken vigorously for 30 s to generate aqueous foam. A small amount of this foam was transferred using a dropper on to a slide with a well. A cover slip was then placed on top of the slide to seal it. The bottom of the sample was then scanned at room temperature. The 2D image stacks were acquired by the software for different z-positions as the probe scanned the sample vertically. The image resolution was 512×512 pixels. The final image processing was performed using Fiji software [33]. The 3d reconstruction of z-stack images was performed to visualize the rendered volume. To obtain the air-bubble image, first an invert function was used on all the images and then the inbuilt plugin 3D Viewer was used to render the volume for 3D viewing. The use of CLSM provides novel insight into the mechanism of particle-stabilized foams or emulsions [34,35].

2.5. Preparation of 2D heterogeneous sandpack

An in-house sandpack holder made of stainless steel was fabricated with one face made of a transparent acrylic plate (thickness: 0.75 in.) for visualization. Chemical-resistant O-rings (McMaster-Carr) were used to provide sealing between acrylic and steel face under high pressure. The dimension of the interior of the holder was 5.4 in. × 2.9 in. × 1 in. There were three injection ports on the left side and three production ports on the right side, as shown in Fig. 3. Stainless steel screens (400 mesh) were welded on these ports to prevent sand flow. The holder was packed with two layers of silica sand: the top layer using 40–70 mesh and the bottom layer using 100–120 mesh. The permeability and the porosity of the system was measured to be 14 Darcy and 30%, respectively. The permeability of the top layer was 22.6 Darcy while that of the bottom layer was 3.8 Darcy. The layer permeabilities were measured by flowing water through a 1D tube (1 ft long; 1 in. in diameter) packed with each sand at a time.

2.6. Oil-free foam flow experiments

Foam flow experiments were conducted to investigate the dynamics of foam flow in a heterogeneous porous medium, first in the absence of crude oil. Foams were stabilized by either a surfactant or a surfactant-nanoparticle blend. Petrophysical properties such as porosity and permeability of the sandpack were determined before performing the vacuum saturation with blue-dyed brine at the room temperature. Fig. 3 shows the experimental schematic. Two series-D syringe pumps from Teledyne ISCO (Lincoln, NE) were used in the setup which are capable of low injection rates (as low as 0.001 cc/min). The apparatus was built to co-inject nitrogen gas and aqueous (brine/surfactant/surfactant-nanoparti cle blend) solution through a sandpack (0.6-in. diameter and 6-in. long) to ensure proper mixing and foam generation. The pre-generated foam was then injected through the three ports on the left side of the heterogeneous sandpack. The downstream pressure of the experiment was maintained by a back-pressure regulator (Equilibar, NC and Swagelok, OH) at 110 psi which was installed downstream of the sandpack. The pressure drop across the 2D sandpack was measured using Rosemount differential pressure transducers. An automated data acquisition system (LabView, National Instruments) was used to record the pressure. The experiment was performed at room temperature. The displacement of dyed-brine by injection fluid was captured using a Supereyes® microscope. The image processing was performed using the ImageJ/Fiji software to calculate the sweep efficiency (fraction of the area that is non-blue) as a function of time. For transient analysis, each image was first cropped into two parts — upper layer and the bottom layer. Each image was first converted to an 8-bit image and then a binary image using the threshold function in the ImageJ. It resulted in black [rgb = (0, 0, 0)] and white [rgb = (255, 255, 255)] colors corresponding to the swept and the unswept region, respectively. The 'plot profile' function was then used to track the average foam front. This function takes an average of the rgb values at yz-planes for every x.

2.7. Oil displacement experiments

The objective of oil displacement experiments was to visualize foam flow behavior in the presence of a crude oil in a heterogeneous system. The same experimental setup was used as in the case of oil-free foam flow experiments and the experiment was performed at room temperature. Conventionally, in such experiments, the oil saturation is performed by displacing the brine-saturated porous media with crude oil at a constant high pressure. However, due to the high permeability contrast (6:1) in the present system, it was not possible to achieve high initial oil saturation using this technique. Therefore, the initial oil saturation was achieved by vacuum saturation which resulted in 100% initial oil saturation for every case. The whole setup was then pressurized with a back pressure of 110 psi. The brine flood was then conducted at 10 ft/D for 4 PV until no oil was produced. Nitrogen gas and surfactant or surfactant-NP blend were then co-injected through sand pack to make a foam at 80% quality (volume fraction of gas). This foam was injected into the two-layer sand pack at an average interstitial velocity of 4 ft/D. This pre-generated foam was injected through the three ports on the left side of the heterogeneous sandpack for more than 18 PV. Oil recovery and pressure

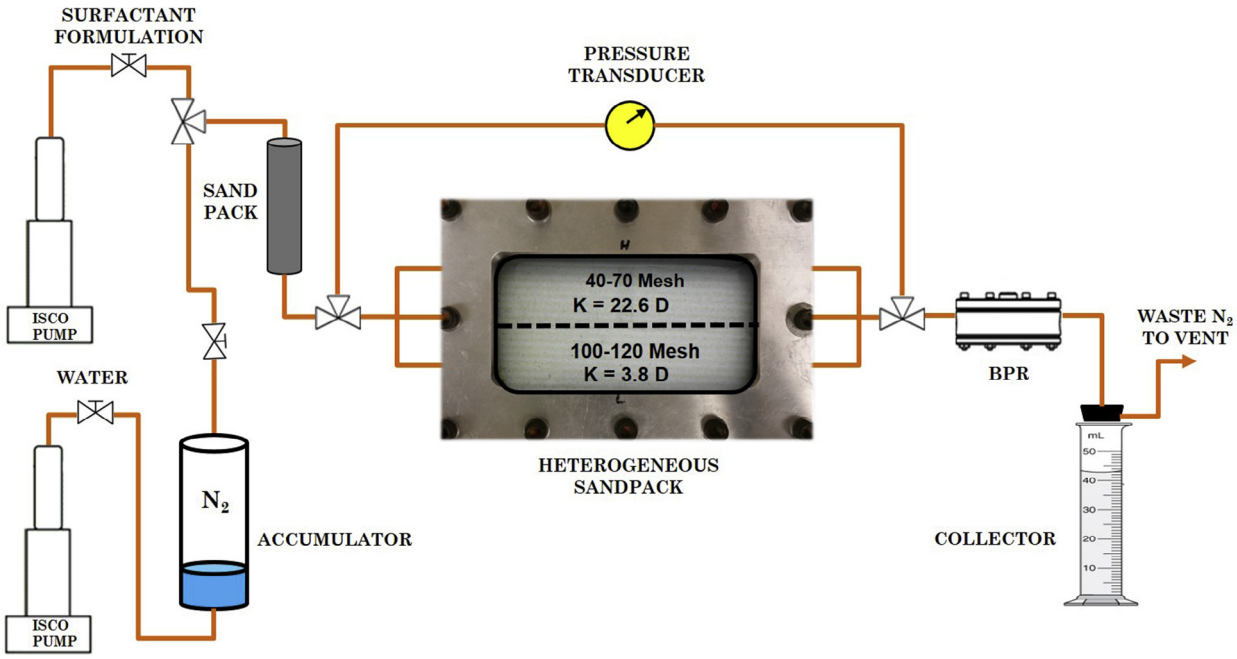

Fig. 3. Schematic of the apparatus for foam flow and oil displacement experiments.

drops were monitored at each step. The oil displacement was captured using a Supereyes® microscope.

3. Results

3.1. Static foam tests

In our previous work [36], we demonstrated that half-lives (time corresponding to 0.5 relative foam height) of static foams stabilized by 0.5 wt% AOS increases from 48 h to more than 4 days by addition of silica nanoparticles (0.3 wt%) at ambient conditions. In this work, similar static foam tests were conducted at higher temperatures (55 °C and 75 °C) to compare the foamability of 0.5 wt% of surfactant with and without nanoparticles. The nanoparticles concentration was kept 0.3 wt% as in our previous study. Since these tests were performed at a higher temperature, evaporation effects were needed to be minimized. So, a setup was used that can provide leak-proof connections. As the dimensions of the cylinder, needle diameter of the air dispenser and amount of liquid initially used were different as compared to the previous setup, the results of these tests should not be compared directly with results from the previous study. Fig. 4 shows the foam decay profile for the surfactant and surfactant-NP blend at 55 °C and 75 °C. The y-axis corresponds to the normalized foam height as a function of time. The foam decayed at a much faster rate at higher temperatures than at the room temperature because of the viscosity reduction of the bulk solution. However, it was observed that with the presence of nanoparticles, half-lives of foam were increased considerably for each temperature case. In our previous study [27], we discussed the mechanisms by which hydrophilic nanoparticles can increase the stability of surfactant-stabilized foam. These includes particle detachment energy [37], maximum capillary pressure of coalescence [38], and kinetics of film drainage [39].

3.2. Confocal laser scanning microscopy (CLSM)

In order to investigate the mechanisms by which nanoparticles enhance surfactant-stabilized foam, CLSM was performed using hydrophilic, fluorescently-tagged silica nanoparticles (FL-NP). A mixture of AOS surfactant (0.5 wt%) and FL-NP (0.3 wt%) was placed in a glass vial and was hand-shaken for 30 s to generate foam with a fine texture. A small amount of this foam was transferred to a slide with a well and CLSM was performed. In this experiment, since the resolution was in the order of microns, it was not possible to resolve individual NP size. However, the microscope can detect the fluorescence emitted from the FL-NP and thus could be used to track the nanoparticles' location in the foam phase. Fig. 5a shows one of the 2d-stack image acquired during the experiment. The yellow fluorescent color indicates the presence of the nanoparticles around the bubbles (black region). These nanoparticles can be seen present uniformly in the bulk liquid phase with no special affinity to the air–water interface due to their hydrophilic nature. A 3d reconstruction of the images was performed using a series of such 2D image stacks (Fig. 5b). A similar 3d reconstruction of the inverted image shows the different bubbles present in the mapped cuboid (Fig. 5c). It can be seen that these nanoparticles form a physical barrier all-around the air-bubble. These closely-packed nanoparticles act a 'colloidal armor' which retard the bubble coalescence and coarsening process. In the literature, several experimental studies have reported this phenomenon where particle-stabilized bubbles are stable (against collapse) for days or weeks as compared to surfactant-stabilized bubbles that collapse in order of hours [40–42]. Note that in the static foam tests and CLSM, we focused on bulk foam stability. In the subsequent sections, we will focus on foam stability in porous media.

3.3. Oil-free foam flow experiments

The objective of foam flow experiments was to investigate the foam rheology in the absence of oil and to visualize the displacement of water by foam in the two-layer model. The layered sand-pack was first fully saturated with blue-dyed water (1 wt% NaCl) by flushing several pore volumes of this fluid. First, a base case was performed in which only brine (1 wt% NaCl) was injected as the displacing fluid at 10 ft/D. Fig. 6 shows the displacement profile as a function of PV injection. The upstream dead volume was equal to 0.09 PV. The reported pore volumes of injection in this paper are after correcting for this dead volume. The injected brine first swept the top layer and a breakthrough was observed in the top layer before it started sweeping the bottom layer. It is to be noted that mobility ratio is 1 for this case. The pressure drop in this case was very low (0.04 psi). The system was again flushed with 20 PV of blue-dyed brine (1 wt% NaCl) to displace the colorless brine before starting the next experiment.

Second, AOS surfactant solution (0.5 wt%) and nitrogen gas were co-injected at 80% quality. Initially, the in-situ generated

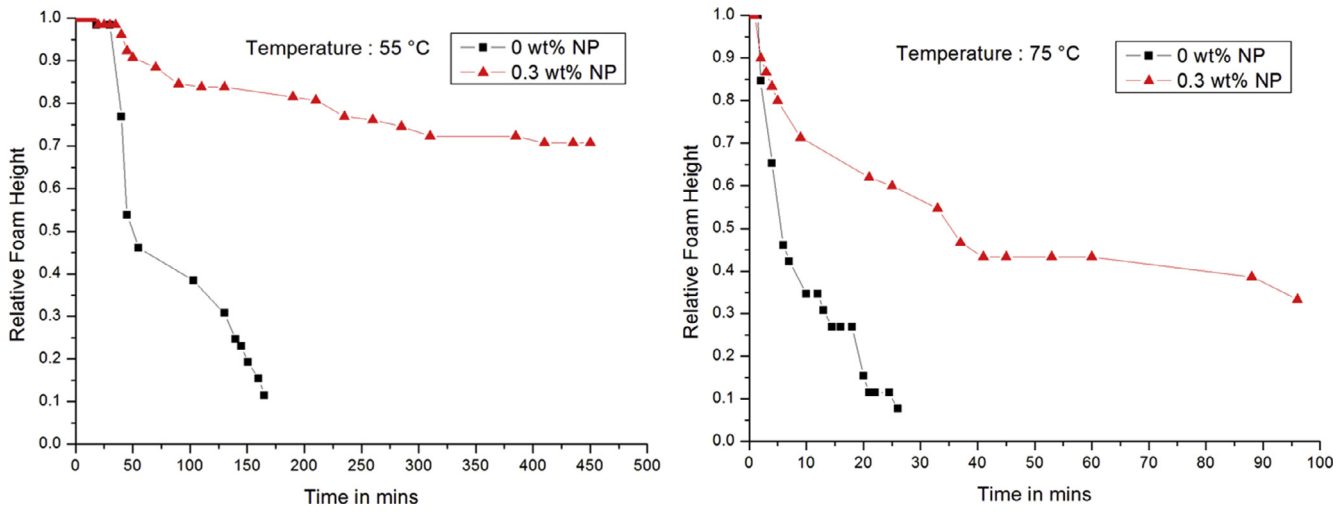

Fig. 4. Static foam tests with and without nanoparticles at 55 °C (left) and 75 °C (right).

foam mixes with the initially 100% water saturated layers. The presence of excess water results in low-quality (less gas fraction by volume), weak foam. The dilution of surfactant at the foam front further weakens the foam. Some of the foam broke down to release gas. Due to a large permeability at the top, significant vertical permeability of the system and the lower density of gas (compared to brine), severe gas channeling was observed from the top of the upper layer. (This channeling was not visible in the displacement profile but was verified by visual inspection of the gas coming out from the outlet). The gas breakthrough was observed in less

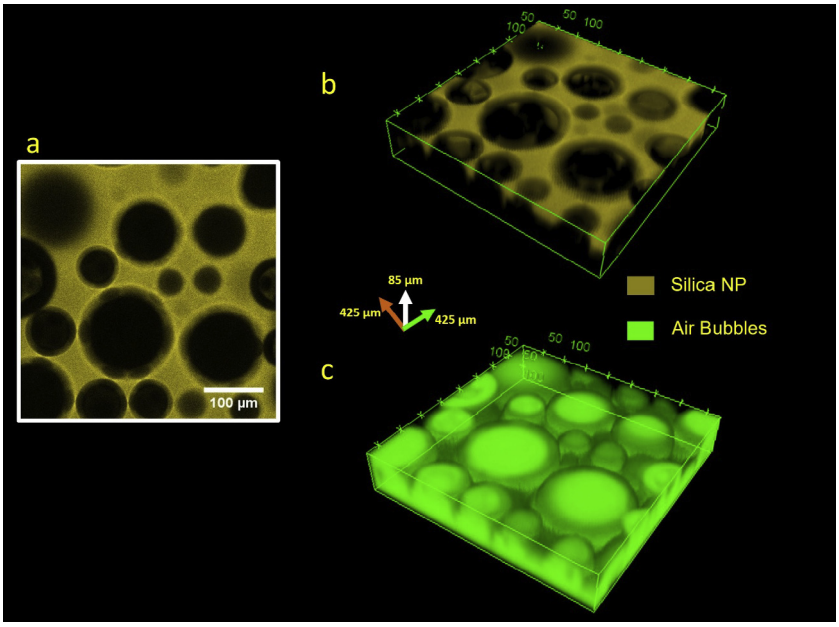

Fig. 5. Confocal laser scanning microscopy images of foams stabilized by 0.5 wt% surfactant and 0.3 wt% FL-NPs: a) 2D stack image showing nanoparticles (yellow) and air bubbles (black); b) 3d reconstructed image showing nanoparticles (yellow); c) 3d reconstructed image showing air bubbles (green). (For interpretation of the references to colour in this figure legend, the reader is referred to the web version of this article.)

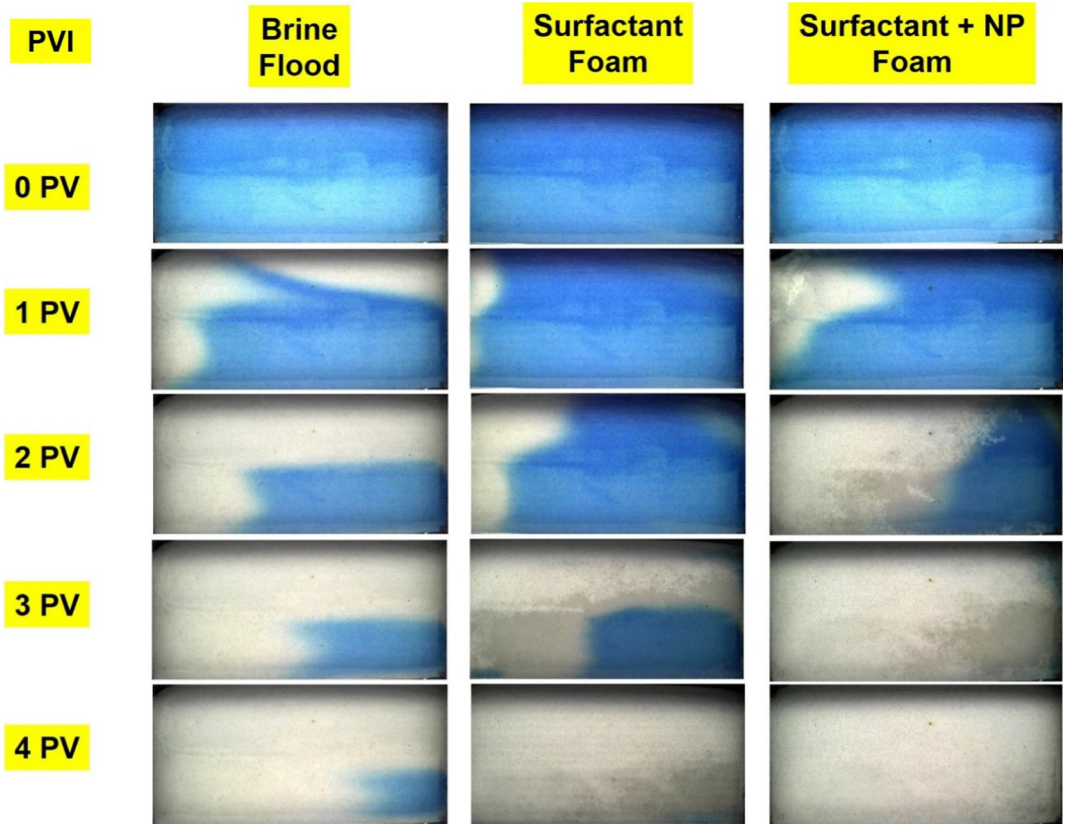

Fig. 6. Displacement profile at different pore volumes of injection (PVI).

than 0.1 pore volume (PV) of foam injection. Even after 1 PV of foam injection, the sweep efficiency was poor and minimal sweep was observed in the low-permeability layer. The initial mobility ratio, M (ratio of mobility of gas to the mobility of the displaced phase) in this case was high compared to the first case of brine flood where M was 1. Therefore, initially sweep efficiency of brine flood was better than that of foam flood. After 1 PV of foam injection, as foam strength increased (and mobility ratio decreased) it started diverting fluid to the low permeability (lower) layer. Note that at this stage, foam had not swept the upper layer completely, but it had started to sweep the bottom layer (as opposed to the brine case). This (sweeping of the low permeability layer before total sweep of the high low permeability layer) is one of the fundamental differences between the sweeping mechanism of foam flooding as compared to any other single-phase injection such as brine, polymer, or surfactant flood. A sweep efficiency of 100% was achieved after 3.75 PV injection. The pressure drop increased from 0.04 psi to 9.3 psi at the end of the experiment. This increase in pressure drop is an indication of strong in-situ foam presence in the system. The resistance factor (RF) which is the ratio of pressure drop due to single-phase brine injection to the pressure drop due to foam injection at the end of experiment was 232.

After the experiment, the system was flushed with 20 PV of methanol to break the foam completely. It was followed by an injection of more than 30 PV of brine (4 wt% NaCl) to flush the methanol. The system was intermittently pressurized and depressurized to remove any trapped gas from the system. The system was again flushed with 20 PV of blue-dyed brine (1 wt% NaCl) to displace the colorless brine before starting the next experiment. To ensure complete removal of the colorless brine, the salinity of the effluent was measured using a handheld analog refractometer which came out to be 1 wt% NaCl (equal to blue-dyed brine). The pressure drop across the sandpack was measured for blue-dyed brine injection at 10 ft/D and it was equal to the initial pressure-drop of brine flood which suggested that no foam is trapped in the system.

The sweep improvement due to foam injection is a strong function of the surfactant formulation. The foaming tendency of the formulation could be increased by either increasing surfactant concentration, adding foam boosters such as zwitterionic surfactants [11] or surface-modified nanoparticles [25,27] or polymers [43]. In this work, we focused on utilizing the synergy between surfactants and hydrophilic nanoparticles in stabilizing foams. Therefore,

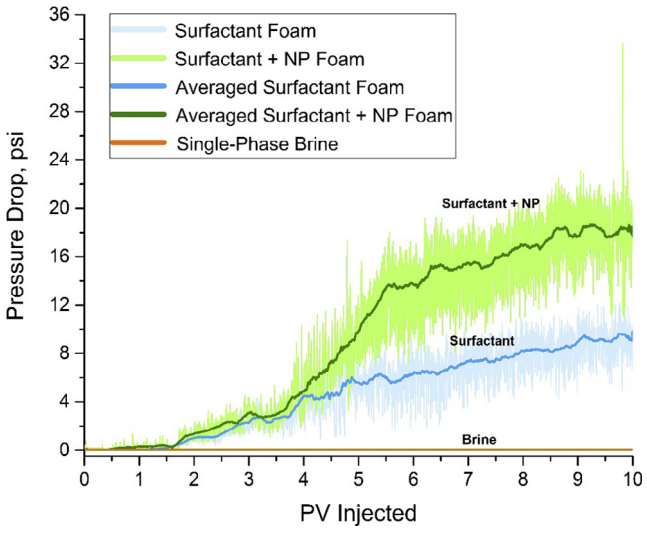

Fig. 7. Pressure drop profiles during foam flow experiments.

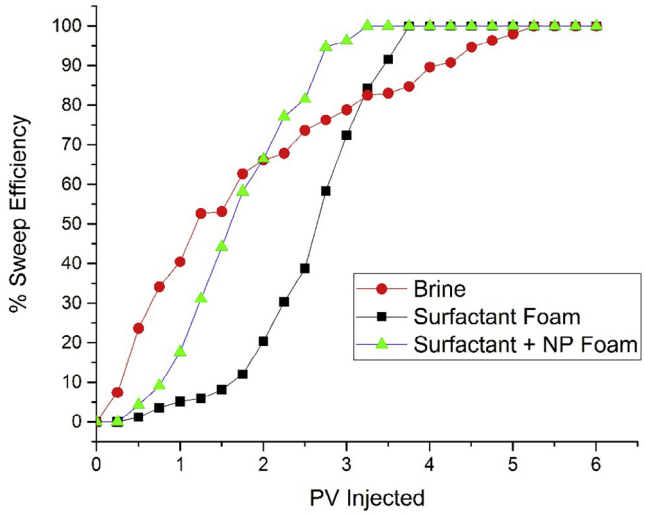

Fig. 8. Plot of sweep efficiency as a function of pore volumes (PV).

a blend of 0.5 wt% AOS surfactant and 0.3 wt% NP was prepared. This blend was co-injected with nitrogen gas at 80% quality. Figs. 7 and 8 shows the comparison of pressure drop and sweep efficiency for the three cases, respectively. For 1 PV of injection – the sweep efficiency of the blend case was better than that of the surfactant case (Fig. 6). It suggests that stronger foam was created faster in the blend case. A 100% sweep efficiency was achieved in about 3 PV for the case of blend foam compared to 4 PV for the case of surfactant foam. The slow foam strengthening for surfactant foam is an impediment for field application and nanoparticles can help lessen its effect. The pressure drop in this case at the end of 10 PV was about 18.2 psi which is 1.95 times the surfactant case, suggesting that the high resistance factor was achieved due to nanoparticles. The RF in this case was 455. Thus, this experiment shows the synergistic interactions of surfactant and nanoparticles in stabilizing foam in a two-layered system. The transient foam flow analysis is discussed in the discussion section.

3.4. Oil displacement experiments

Flood 1 was conducted with the surfactant AOS as the foaming agent. The porosity and permeability of the two-layer sandpack were 30% and 14 Darcy, respectively. The sandpack was vacuum-saturated with crude oil which resulted in the initial oil saturation of 100%. Fig. 9 shows the injection schedule, cumulative oil recovery (secondary y-axis) and overall pressure drop (primary y-axis) across the sandpack. Brine flood was conducted at 10 ft/D to mimic a waterflood in a reservoir. It was continued for more than 4 PV until no oil was produced. The waterflood oil recovery was 46% OOIP (original oil in place) and oil saturation was reduced to 54%. The pressure drop during water flood was very low (0.17 psi).

Fig. 10 shows the oil distribution during foam flooding at different pore volumes of injection. Water flood swept only the top high-permeability layer, leaving all the oil in the bottom low-permeability layer (Fig. 10A). It is interesting to note that at this stage adopting any other tertiary recovery process such as gas flooding, surfactant flooding or polymer flooding will result in channeling of injection fluid in the top layer. However, foam has the capability to divert flow from high permeability region to low permeability region. Therefore, this water flood was followed by a foam flood. AOS surfactant solution (0.5 wt%) and nitrogen gas were coinjected with a quality of 80% at 4 ft/D. Fig. 10B shows the foam flow diversion from the high-permeability layer to the low-permeability layer. Foam flood increased the oil recovery by

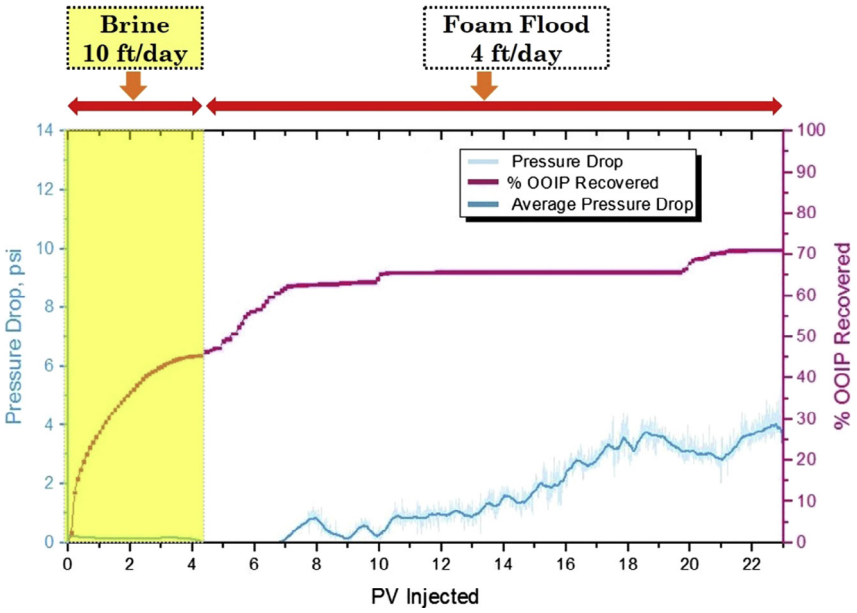

Fig. 9. Pressure drop profile (cyan, left axis) and cumulative oil recovery (pink, right axis) for Flood 1. (For interpretation of the references to colour in this figure legend, the reader is referred to the web version of this article.)

17% within the first 4.5 PV. The oil recovery almost plateaued after 8 PVI, which is in agreement with the observed oil distribution (Figs. 10C,D,E) in which no substantial sweep efficiency was achieved between 6 and 14 PV. The remaining oil slowly came out primarily due to crossflow of oil from the low-permeability to the high-permeability region as seen in Figs. 10D and E. The pressure drop started to increase after 1.5 PV of foam injection and reached a value of 4 psi (compared to 0.17 psi for waterflood). The ultimate cumulative oil recovery was 71.1% OOIP, the incremental oil recovery by foam was 25.1% OOIP and the final oil saturation was 28.9%. It took 23 PV to reach this state.

Flood 2 was conducted with a blend of surfactant (AOS) and nanoparticles as the foaming agent. The sandpack holder was again packed with clean oil-free sand. The same porosity and permeability of the system were achieved as in the previous flood. The sandpack was then vacuum-saturated with crude oil resulting in the initial oil saturation of 100%. Fig. 11 shows the injection procedure, cumulative oil recovery (secondary y-axis) and overall pressure drop (primary y-axis) across the sandpack. Similar to Flood 1, first a brine flood was conducted at 10 ft/D. It was continued for more than 4 PV until oil production significantly slowed down. The waterflood oil recovery was 45% OOIP and oil saturation was reduced to 55% which is similar to the Flood 1 result. Then, a surfactant-nanoparticle blend (0.5 wt% AOS + 0.3 wt% NP) and nitrogen gas was coinjected with a quality of 80% at 4 ft/D. Fig. 10 shows the comparison of oil distribution due to foam flooding at different pore volumes (PV) of injection for the surfactant case (left) and the blend case (right). Foam flow diversion can be seen from the high-permeability layer to the lower one (Fig. 10H). Foam flood increased the oil recovery to 62% OOIP within the first 4.5 PV. A close to 100% sweep was observed in about 10 PV (compared to 18 PV for surfactant foam case). Note that a large amount of oil still came out even after 10 PVI. The reason for this is that even if the foam/gas sweeps a certain region, it has non-zero residual oil saturation which could be further reduced by foam. This left-behind oil in the swept region could not be seen by the eye. The pressure drop started to increase after 1 PV of foam injection and reached a value of 5 psi (compared to 0.17 psi for waterflood). The oil recovery in the blend case increased continuously as opposed to the case of surfactant foam which almost plateaued after 10 PVI. The higher oil recovery in this case could be attributed to better microscopic as well as volumetric sweep efficiency due to stronger in-situ nanoparticle-stabilized foam. The ultimate cumulative oil recovery (after 22 PV) was 79.4% OOIP; incremental oil recovery by foam was 34.4% and final oil saturation was 20.6%.

4. Discussion

4.1. Effect of nanoparticles

An image analysis was performed on the pictures of transient foam flow in the absence of oil. Fig. 12 shows the foam front profiles in the surfactant and surfactant-np cases. The different plots correspond to different pore volumes of injection. The x-axis represents the normalized spatial horizontal length along the sandpack. The y-axis represents the unswept fraction in the yz-plane at any x. Fig. 12 shows that, for the case of surfactant, up to 2.5 PV of foam injection the foam fronts in the top (Fig. 12A) and bottom layer (Fig. 12B) move at different speeds with the foam front in the bottom (low-permeability) layer lagging. For the same 2.5 PV of foam injection in the case of the blend, foam fronts move at the same speed (Fig. 12C,D). This shows that due to the presence of nanoparticles, stronger in-situ foam was generated in the top layer which effectively diverted foam in the low permeability region faster. In our previous study [27], we reported such synergistic stabilization of foam by the surfactant-nanoparticle blend in one-dimensional homogenous media. The effect of stabilization on volumetric sweep is demonstrated in the present multi-dimensional system. The presence of nanoparticles increases the in-situ foam strength in both high and low permeability layers (but disproportionately) which result in an effective sweep. The other implication of these results is that foam in a heterogeneous system where layers are in capillary contact tends to self-regulate its mobility in each layer. Similar observations have been reported in the literature [44].

4.2. Foam phase separation

Khatib et al. (1988) introduced the concept of limiting capillary pressure, P_C^* for foam in porous media. It is the capillary pressure

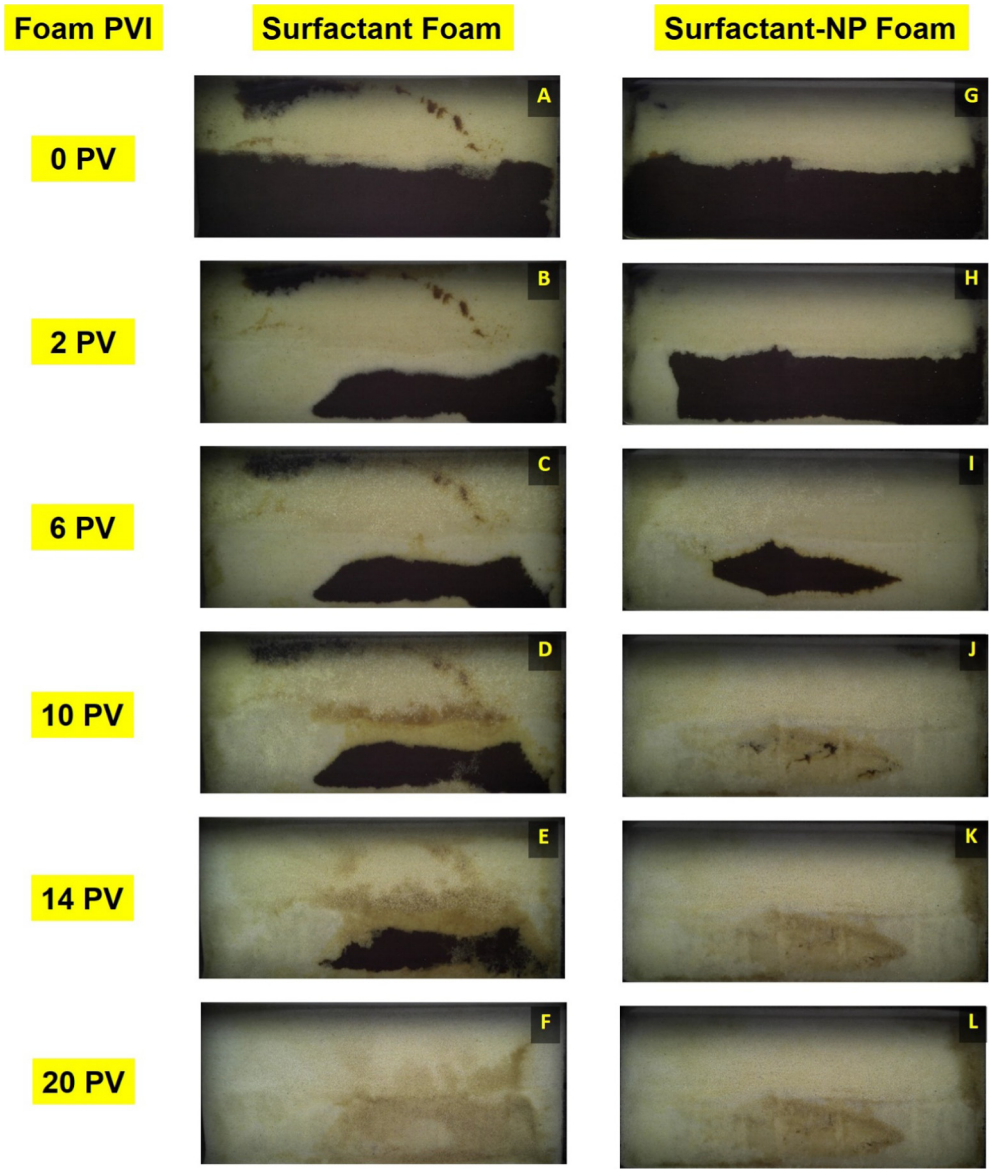

Fig. 10. Oil distributions during Flood 1 (left) and Flood 2 (right) at different pore volumes of foam injection (PVI).

above which foam collapses abruptly. It is analogous to critical disjoining pressure in bulk foam above which lamellae collapse [45]. P_C^* is a function of surfactant type and concentration, salt concentration, gas flow rate, and porous media permeability [46]. In the present heterogeneous layered system, both layers will have different P_C^*. Literature data suggests that limiting capillary pressure increases with a decrease in permeability [47]. Therefore, the layer with higher value of P_c^* (bottom low-permeability layer in this case) will draw water from the layer with lower value of P_c^* (upper high-permeability layer) [48]. In our foam flow experiments, we visualized this phenomenon during foam injection where the surfactant solution entered the low-permeability region first followed by the foam. Fig. 13 shows the displacement profile at 3.2 PV of surfactant foam injection. Based on the color, it can be seen that it is the liquid fraction of the foam that initially enters the low-permeability region which is later followed by foam. This suggest that capillary crossflow in the present case weakens the foam in the high-permeability layer particularly near the boundary of abrupt permeability contrast. Thus, this phenomenon works antagonistically towards improving the flow diversion due to foam. These observations suggest that special care must be taken during foam simulation in layered system such as optimal grid-size selection to capture this effect near the boundary. Foam phase separation in such systems is one of the key mechanisms and the assumption that foam will stay as a homogeneous "foam" phase should not be made in simulations.

4.3. Crossflow

Two types of cross-flow behavior were distinctly observed during foam (both surfactant and blend case) flood in the oil displacement experiments. The first cross-flow type was observed in which foam diversion happens from the high-permeability layer to the low-permeability layer as shown in Fig. 14A. This flow diversion is due to the fact that foam strength increases in high-permeability layer more than that in lower-permeability layer [44,49]. This selective mobility reduction is a known attribute of foam flow in heterogeneous porous system which helps to improve the volumetric sweep [50]. The second type of cross-flow was the flow of oil from the low-permeability layer to the

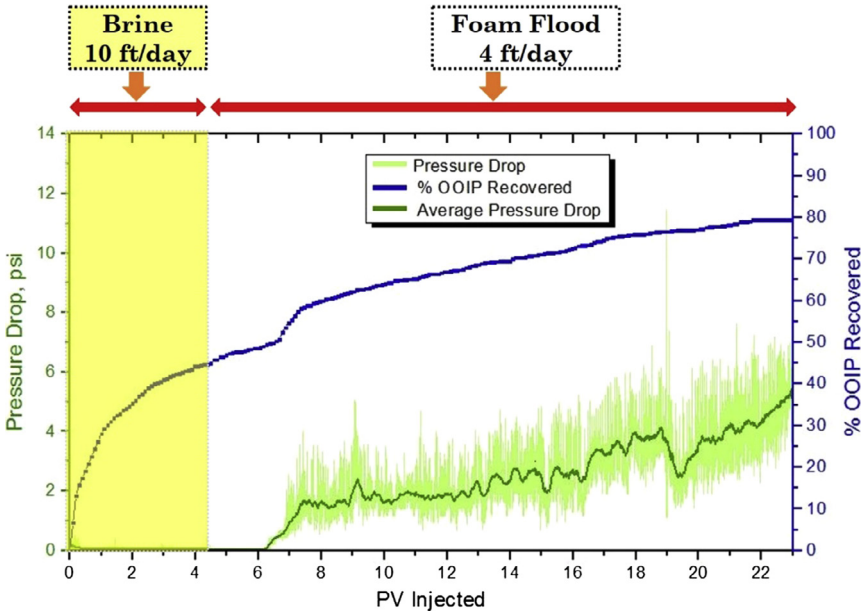

Fig. 11. Pressure drop profile (green, left axis) and cumulative oil recovery (blue, right axis) for Flood 2. (For interpretation of the references to colour in this figure legend, the reader is referred to the web version of this article.)

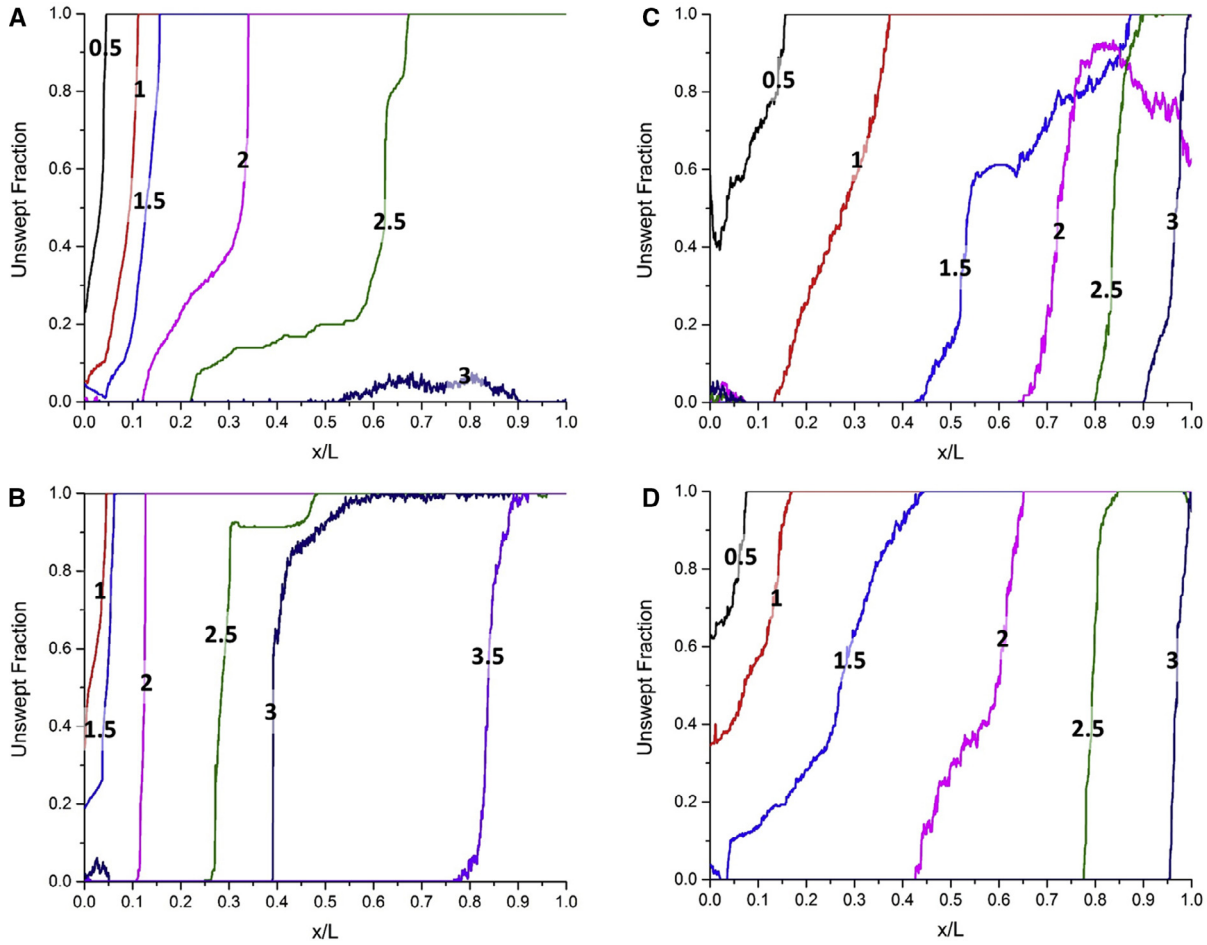

Fig. 12. Sweep profiles in the top (A, C) and bottom layers (B, D) of sandpack during foam flow experiments at different pore volumes (labeled on curves) for: surfactant foam case (left); surfactant-np blend foam case (right).

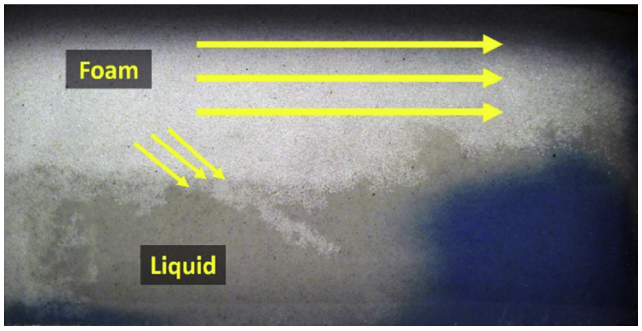

Fig. 13. Foam phase separation during foam flow experiment.

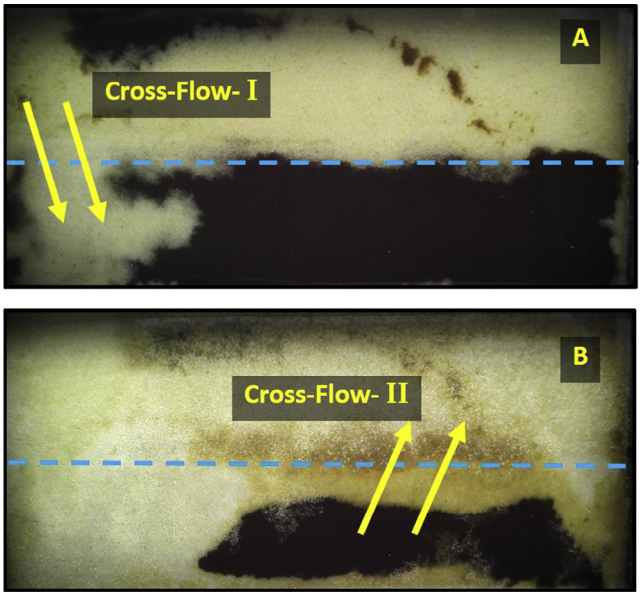

Fig. 14. Two types of cross-flow mechanisms observed during oil displacement experiments.

high-permeability layer, as shown in Fig. 14B. If the permeability contrast is significant, it is easier for oil to flow out through the upper layer than the lower layer. Simulations should capture both cross-flow behaviors.

5. Conclusion

The following conclusions can be drawn from this work:

- Static foam tests show the synergistic interaction of surfactant and nanoparticles on foam stability. The half-lives of the foam increase due to the presence of nanoparticles at both 55 °C and 75 °C.
- Confocal laser scanning microscopy revealed that nanoparticles form a physical barrier in the liquid film between two air-bubbles which enhances the foam stability.
- Despite the presence of a permeability contrast (6:1), which is favorable of channeling of gas through high permeability region, foam was effective in diverting fluid to low-permeability region irrespective of the presence of crude oil.
- Foam flow experiments showed that the liquid fraction of the foam is first diverted to the low-permeability layer followed by the whole foam. It suggests that foam cannot be always treated as a homogeneous "foam" phase during foam flow in a heterogeneous system.
- Foam flood in heterogeneous sandpacks with a reservoir crude oil showed that incremental oil recovery of 25%–34% OOIP (over waterflood) using immiscible foams. Foams stabilized by surfactant-nanoparticle blend outperform surfactant-stabilized foam by 9% OOIP.
- Two different types of cross-flow between the low-permeability layer and the high-permeability layer were identified as key mechanisms governing oil-displacement process during foam flooding process.

In summary, we showed that synergistic stabilization of foams via surfactant and nanoparticles improves the sweep efficiency in a heterogeneous system with and without the presence of crude oil. This study shows that hydrophilic nanoparticles have an immense potential to increase the robustness of surfactant-stabilized foams in subsurface applications.

Acknowledgment

We are thankful to the sponsors of Gas EOR Industrial Affiliates Project at The University of Texas at Austin for partial funding of this work. We would also like to thank Julie Hayes for assisting us with the confocal laser scanning microscopy.

References

[1] Worldwide EOR survey. Oil Gas J 2014;112(4).
[2] Lake LW. Enhanced oil recovery. Englewood Cliffs, NJ: Prentice Hall; 1989.
[3] Rossen WR. Foams in enhanced oil recovery. Surfactant Sci Ser 1996:413–64.
[4] Kovscek AR, Tadeusz WP, Radke CJ. Mechanistic foam flow simulation in heterogeneous and multidimensional porous media. SPE J 1997;2(4):511–26.
[5] Rossen WR, Van Duijn CJ, Nguyen QP, Shen C, Vikingstad AK. Injection strategies to overcome gravity segregation in simultaneous gas and water injection into homogeneous reservoirs. SPE J 2010;15(1):76–90.
[6] Bernard GG, Jacobs WL. Effect of foam on trapped gas saturation and on permeability of porous media to water. Soc Petrol Eng J 1965;5(4):295–300.
[7] Patzek TW. Field applications of steam foam for mobility improvement and profile control. SPE Reserv Eng 1996;11(2):79–86.
[8] Blaker T et al. Foam for gas mobility control in the Snorre field: the FAWAG project. SPE Reserv Eval Eng 2002;5(4):317–23.
[9] Chou SI, Vasicek SL, Pisio DL, Jasek DE, Goodgame JA. CO_2 foam field trial at north ward-estes, In: SPE annual technical conference and exhibition, 4–7 October, Washington, D.C., SPE-24643; 1992.
[10] Mukherjee J, Nguyen QP, Scherlin J, Vanderwal P, Rozowski P. CO_2 foam pilot in salt creek field, Natrona county, WY: phase III: analysis of pilot performance, In: SPE improved oil recovery conference, 11–13 April, Tulsa, Oklahoma, USA, SPE-179635; 2016.
[11] Singh R, Mohanty KK. Foams with wettability-altering capabilities for oil-wet carbonates: a synergistic approach. SPE J 2016;21(4):1126–39.
[12] Sharma H, Dufour S, Arachchilage GWP, Weerasooriya U, Pope GA, Mohanty K. Alternative alkalis for ASP flooding in anhydrite containing oil reservoirs. Fuel 2015;140:407–20.
[13] Ziegler VM, Handy LL. Effect of temperature on surfactant adsorption in porous media. Soc Petrol Eng J 1981;21(2):218–28.
[14] Jensen JA, Friedmann F. Physical and chemical effects of an oil phase on the propagation of foam in porous media, In: SPE california regional meeting, 8–10 April, Ventura, California, SPE-16375; 1987.
[15] Singh R, Mohanty KK. Foams Stabilized by In-Situ Surface-Activated Nanoparticles in Bulk and Porous Media. SPE J 2016;21(1):121–30.
[16] Singh R, Gupta A, Mohanty KK, Huh KK, Lee D, Cho H. Fly ash nanoparticle-stabilized CO_2-in-water foams for gas mobility control applications, In: SPE annual technical conference and exhibition, 28–30 September, Houston, Texas, USA, SPE-175057; 2015.
[17] Lee D, Cho H, Lee J, Huh C, Mohanty K. Fly ash nanoparticles as a CO_2 foam stabilizer. Powder Technol 2015;283:77–84.
[18] Binks BP, Horozov TS. Aqueous foams stabilized solely by silica nanoparticles. Angew Chem 2005;117(24):3788–91.
[19] Stocco A, Rio E, Binks BP, Langevin D. Aqueous foams stabilized solely by particles. Soft Matter 2011;7(4):1260–7.
[20] Yu J, Khalil M, Liu N, Lee R. Effect of particle hydrophobicity on CO_2 foam generation and foam flow behavior in porous media. Fuel 2014;126:104–8.
[21] Gonzenbach UT, Studart AR, Tervoort E, Gauckler LJ. Ultrastable particle-stabilized foams. Angew Chem Int Ed 2006;45(21):3526–30.
[22] Arriaga LR et al. On the long-term stability of foams stabilised by mixtures of nano-particles and oppositely charged short chain surfactants. Soft Matter 2012;8(43):11085–97.

[23] Zhu Y, Pei X, Jiang J, Cui Z, Binks BP. Responsive aqueous foams stabilized by silica nanoparticles hydrophobized in situ with a conventional surfactant. Langmuir 2015;31(47):12937–43.
[24] Worthen AJ, Bagaria HG, Chen Y, Bryant SL, Huh C, Johnston KP. Nanoparticle-stabilized carbon dioxide-in-water foams with fine texture. J Colloid Interface Sci 2013;391:142–51.
[25] Sun Q, Li Z, Li S, Jiang L, Wang J, Wang P. Utilization of surfactant-stabilized foam for enhanced oil recovery by adding nanoparticles. Energy Fuels 2014;28 (4):2384–94.
[26] Zargartalebi M, Kharrat R, Barati N. Enhancement of surfactant flooding performance by the use of silica nanoparticles. Fuel 2015;143:21–7.
[27] Singh R, Mohanty KK. Synergy between nanoparticles and surfactants in stabilizing foams for oil recovery. Energy Fuels 2015;29(2):467–79.
[28] Conn CA, Ma K, Hirasaki GJ, Biswal SL. Visualizing oil displacement with foam in a microfluidic device with permeability contrast. Lab Chip 2014;14 (20):3968–77.
[29] Caldelas FM, Murphy M, Huh C, Bryant SL. Factors governing distance of nanoparticle propagation in porous media, In: SPE production and operations symposium, 27–29 March, Oklahoma City, Oklahoma, USA, SPE-142305; 2011.
[30] Cumberland SA, Lead JR. Particle size distributions of silver nanoparticles at environmentally relevant conditions. J Chromatogr A 2009;1216 (52):9099–105.
[31] Vikingstad AK, Skauge A, Høiland H, Aarra M. Foam–oil interactions analyzed by static foam tests. Colloids Surf 2005;260(1):189–98.
[32] Jones SA, van der Bent V, Farajzadeh R, Rossen WR, Vincent-Bonnieu S. Surfactant screening for foam EOR: correlation between bulk and core-flood experiments. Colloids Surf 2016;500:166–76.
[33] Schindelin J et al. Fiji: an open-source platform for biological-image analysis. Nat Methods 2012;9(7):676–82.
[34] Murray BS, Durga K, Yusoff A, Stoyanov SD. Stabilization of foams and emulsions by mixtures of surface active food-grade particles and proteins. Food Hydrocolloids 2011;25(4):627–38.
[35] Zou S, Yang Y, Liu H, Wang C. Synergistic stabilization and tunable structures of pickering high internal phase emulsions by nanoparticles and surfactants. Colloids Surf A 2013;436:1–9.
[36] Singh R, Mohanty KK. Synergistic stabilization of foams by a mixture of nanoparticles and surfactants, In: SPE improved oil recovery symposium, 12–16 April, Tulsa, Oklahoma, USA, SPE-169126; 2014.
[37] Binks BP. Particles as surfactants—similarities and differences. Curr Opin Colloid Interface Sci 2002;7(1–2):21–41.
[38] Pugh RJ. Foaming, foam films, antifoaming and defoaming. Adv Colloid Interface Sci 1996;64:67–142.
[39] Horozov TS. Foams and foam films stabilised by solid particles. Curr Opin Colloid Interface Sci 2008;13(3):134–40.
[40] Du Z, Bilbao-Montoya MP, Binks BP, Dickinson E, Ettelaie R, Murray BS. Outstanding stability of particle-stabilized bubbles. Langmuir 2003;19 (8):3106–8.
[41] Subramaniam AB, Mejean C, Abkarian M, Stone HA. Microstructure, morphology, and lifetime of armored bubbles exposed to surfactants. Langmuir 2006;22(14):5986–90.
[42] Kostakis T, Ettelaie R, Murray BS. Enhancement of stability of bubbles to disproportionation using hydrophilic silica particles mixed with surfactants or proteins. Food Colloids 2007:357–68.
[43] Pei H, Zhang G, Ge J, Wang J, Ding J, Liu X. Investigation of polymer-enhanced foam flooding with low gas/liquid ratio for improving heavy oil recovery, In: Canadian unconventional resources and international petroleum conference, 19–21 October, Calgary, Alberta, Canada, SPE-137171; 2010.
[44] Bertin HJ, Apaydin OG, Castanier LM, Kovscek AR. Foam flow in heterogeneous porous media: effect of cross flow. SPE J 1999;4(2):75–82.
[45] Aronson AS, Bergeron V, Fagan ME, Radke CJ. The influence of disjoining pressure on foam stability and flow in porous media. Colloids Surf A 1994;83 (2):109–20.
[46] Khatib ZI, Hirasaki GJ, Falls AH. Effects of capillary pressure on coalescence and phase mobilities in foams flowing through porous media. SPE Reserv Eng 1988;3(3):919–26.
[47] Farajzadeh R, Lotfollahi M, Eftekhari AA, Rossen WR, Hirasaki GJH. Effect of permeability on implicit-texture foam model parameters and the limiting capillary pressure. Energy Fuels 2015;29(5):3011–8.
[48] Rossen WR, Lu Q. Effect of capillary crossflow on foam improved oil recovery, In: presented at the SPE western regional meeting, 25–27 June, Long Beach, California, SPE-38319; 1997.
[49] Casteel JF, Djabbarah NF. Sweep improvement in CO_2 flooding by use of foaming agents. SPE Reserv Eng 1988;3(4):1186–92.
[50] Heller JP. CO_2 foams in enhanced oil recovery. Adv Chem Ser 1994;242: 201.